ECS Transactions, 25 (34) 3-13 (2010)
10.1149/1.3335487 ©The Electrochemical Society

2D Nucleation and Growth Phenomena in UPD of Cd on Ag(111) and Ag(100)

G. Staikov[a], S. G. García[b], and D. R. Salinas[b]

[a] Institute of Solid State Research (IFF-6), Research Centre Jülich, 52425 Jülich, Germany
[b] INIEC-Dpto. de Ingeniería Química, Universidad Nacional del Sur, 8000 Bahía Blanca, Argentina

Underpotential deposition (UPD) of Cd on Ag single crystal substrates has been studied by in situ scanning tunneling microscopy (STM) and electrochemical measurements. On Ag(111) the UPD process starts with formation of an expanded adlayer with a $Ag(111)-(\sqrt{3}\times\sqrt{19})R23.4°$ superlattice structure. In the UPD range $50\,\mathrm{mV} < \Delta E < 80\,\mathrm{mV}$ this adlayer transforms by 2D nucleation and growth to a condensed Cd monolayer, which is unstable and at long polarization times undergoes changes involving surface alloy formation phenomena. In contrast to Ag(111), on Ag(100) a formation of a condensed monolayer by 2D nucleation and growth has been observed at relatively high underpotentials ($130\,\mathrm{mV} \le \Delta E \le 180\,\mathrm{mV}$). The growth rate of 2D clusters extracted from the in situ STM images indicates a surface diffusion-controlled growth kinetics. At lower underpotentials the UPD of Cd on both substrates involves a significant surface alloy formation, which is reflected in the surface topography changes observed during the anodic stripping.

Introduction

Two-dimensional (2D) nucleation and growth processes are observed in both the overpotential deposition (OPD) and the underpotential deposition (UPD) of metals. In the first case 2D nucleation and propagation of separate monolayers are involved in the electrochemical growth of quasi-perfect (screw dislocation free) crystal faces. This crystal growth mechanism has been elegantly demonstrated by Evgeni Budevski and his coworkers in the famous experiments performed on screw dislocation free Ag single crystal faces (1-3). In the case of UPD of metals 2D nucleation and growth phenomena are involved in the formation of condensed metal monolayers on foreign single crystal substrates (3,4). Therefore, the understanding of these phenomena is of great importance for the application of UPD processes for modification of surfaces with ultrathin films and heterostructures.

In this contribution, we present in-situ STM studies of Cd UPD on Ag(111) and Ag(100) substrates. These studies are interesting not only from fundamental point of view but also due to the potential application of Cd UPD processes in the electrochemical atomic layer epitaxy (ECALE) (5,6). Information on the kinetics and mechanism of UPD processes is obtained combining in situ STM observations with voltammetric and transient measurements.

Experimental

The experiments were performed in the systems Ag(111)/Cd^{2+} and Ag(100)/Cd^{2+}. The electrolyte solution (5mM $CdSO_4$ + 5mM H_2SO_4 + 0.5M Na_2SO_4) was prepared from Merck suprapure chemicals and ultrapure water. Before each experiment the surface of single crystal electrodes was mechanically polished and subsequently chemically etched according to a previously described standard procedure (7,8). In situ STM measurements were carried out with standard NanoScopeIII equipment (Digital Instruments, Santa Barbara, CA, USA) using Pt-Ir tips coated with Apiezon wax.

Results and Discussion

The System Ag(111)/Cd^{2+}

Figure 1 shows the cyclic voltammogram (CV) of the system Ag(111)/Cd^{2+} in the underpotential range $\Delta E = E - E_{3DCd} \geq 0$ (E and E_{3DCd} represent the actual electrode potential and the Nernst equilibrium potential of the pure 3D Cd bulk phase, respectively). The voltammogram is characterized by four adsorption(A)/desorption(D) peak pairs. The A_1/D_1 and A_2/D_2 peak pairs are nearly symmetrical, which can be attributed to the occurrence of reversible adsorption/desorption processes. In situ STM imaging with lateral atomic resolution in the underpotential range 100mV ≤ ΔE ≤ 150mV revealed the formation of an expanded adlayer with a $Ag(111)-(\sqrt{3}\times\sqrt{19})R23.4°$ superlattice structure (8). The calculated charge density for the formation of a Cd adlayer with such structure (q_{calc}=111 μC/cm^2) is close to the experimental cathodic charge density ($|\Delta q_{exp}|$≈120 μC/cm^2) obtained from the integration of the cyclic voltammogram in the UPD range 100mV ≤ ΔE ≤ 400mV.

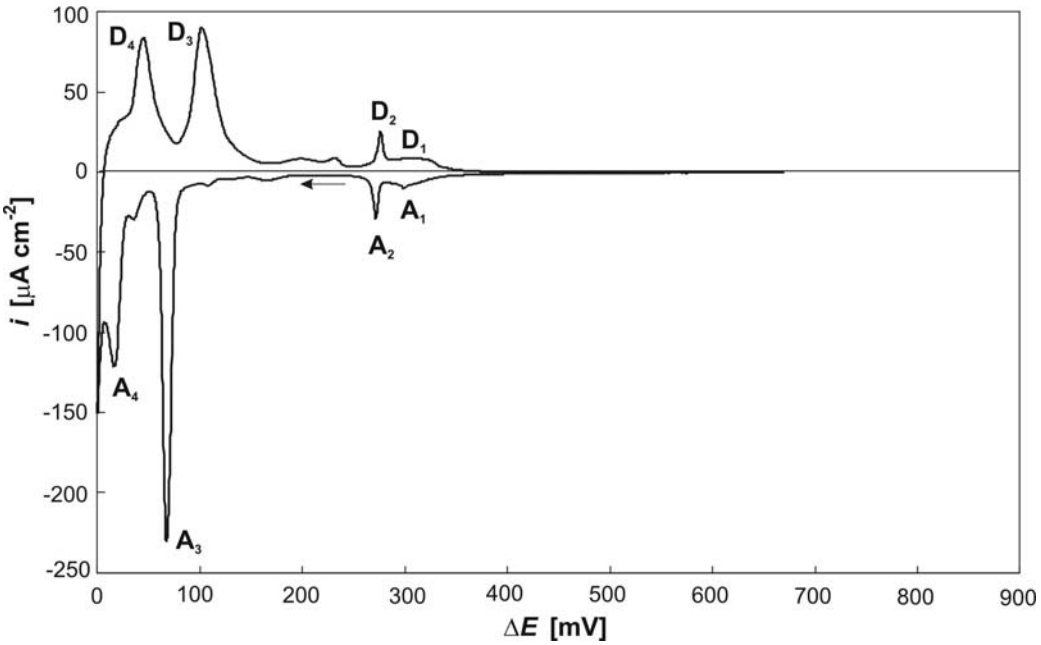

Figure 1. Cyclic voltammogram for Cd UPD in the system Ag(111)/Cd^{2+}(scan rate: |dE/dt| = 10 mV/s).

In situ STM images shown in Figure 2 present the surface topography changes during the UPD of Cd by stepping the underpotential from ΔE=125mV to ΔE=70mV. Figure 2(a) shows the initial surface topography at ΔE=125mV. This surface topography remains unchanged in the UPD range 125mV ≤ ΔE ≤ 400mV, where the formation of the expanded adlayer with the $\mathrm{Ag(111)}-(\sqrt{3}\times\sqrt{19})R23.4°$ superlattice structure occurs. However, a growth front appears in the STM image in Figure 2(b) after stepping the underpotential from ΔE=125mV to ΔE=70mV. This observation gives clear evidence for a transformation of the expanded adlayer to a condensed Cd monolayer by 2D nucleation and growth starting preferentially at substrate monatomic step edges. As seen in Figure 2(c), the nucleation and growth of a 2D Cd cluster on top of the substrate island is delayed, which indicates a higher barrier for 2D nucleation on atomically flat terraces in good agreement with the theoretical predictions (3,4). In the stage corresponding to the STM image in Figure 2(d) the Ag(111) substrate is covered completely by the condensed Cd monolayer and the surface topography is identical with that in Figure 2(a). In situ STM imaging with atomic resolution under these polarization conditions has shown a close-packed 2D atomic structure of the condensed Cd monolayer (8). This observation is in agreement with the experimental cathodic charge density ($|\Delta q_{exp}|\approx$ 410 μC/cm^2) obtained in the UPD range 50mV ≤ ΔE ≤ 400mV.

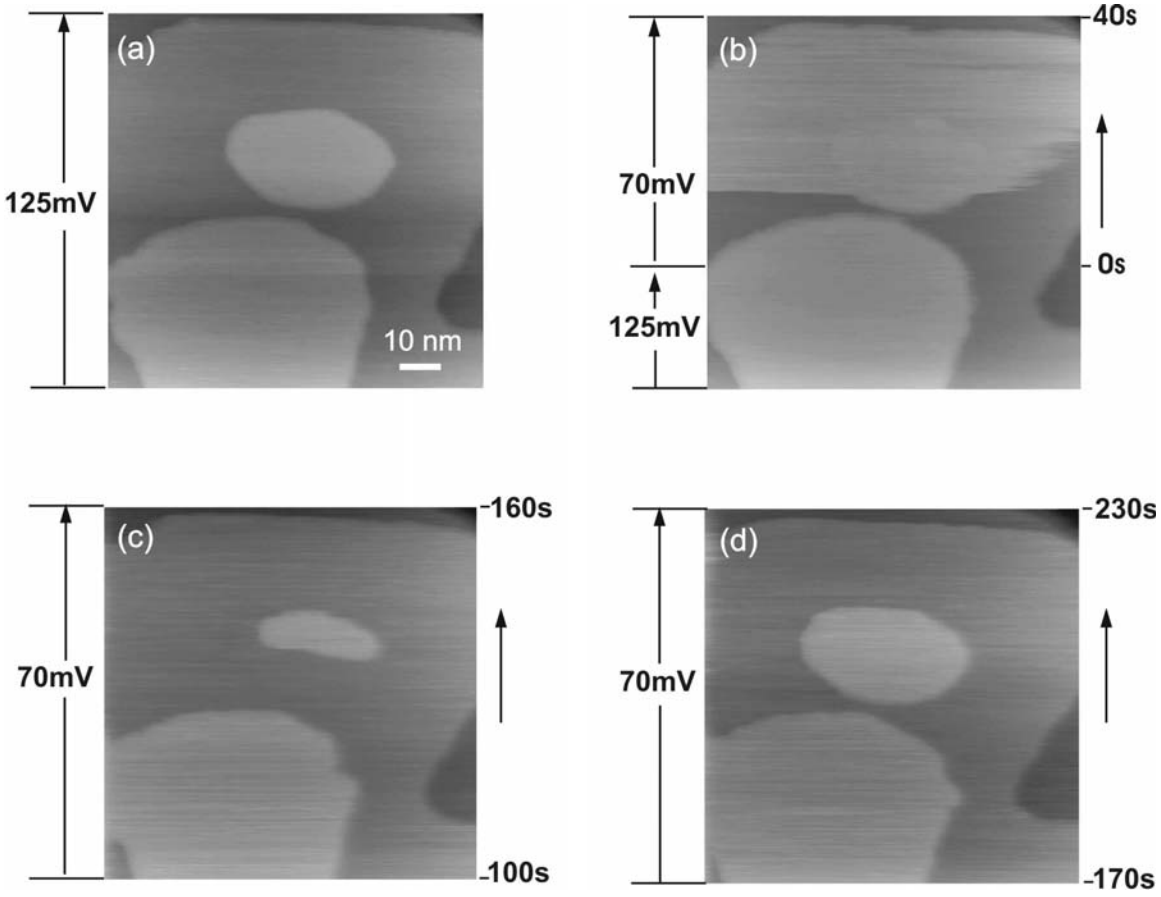

Figure 2. In situ STM images showing the surface topography changes during Cd UPD in the system Ag(111)/Cd^{2+}. (a): Initial surface topography at ΔE=125mV. (b-d): Surface topography changes after a potential step from ΔE=125mV to ΔE=70mV.

Figure 3(a) shows current transients for Cd UPD obtained by stepping the underpotential from ΔE_i=125mV (where the expanded adlayer is completed) to relatively low final underpotentials. The transients exhibit a current maximum $i_m(t_m)$, which is characteristic for a deposition process involving 2D nucleation and growth. However, the non-dimensional i/i_m vs. t/t_m plot of the transients presented in Figure 3(b) shows significant deviation from the theoretical transients predicted by the classical models for instantaneous and progressive 2D nucleation (1-3,9,10). These results indicate that the growth of 2D Cd clusters is slower than expected from the existing theoretical models. Similar results were reported in the case of Rh electrodeposition on Au(100) and were attributed to a decrease of the radial growth rate of the 2D Rh clusters provoked by the presence of various surface inhomogeneities (11). A decrease of the radial growth rate can be expected also in the case of a surface diffusion-controlled growth of 2D clusters (10,12,13). A new model including 2D nucleation and surface diffusion-controlled growth has been developed and applied successfully for the description of current transients for the anodic deposition of a calomel monolayer on mercury (14). The possibility for a description of experimental transients shown in Figure 3(a) on the basis of such a model is presently being examined.

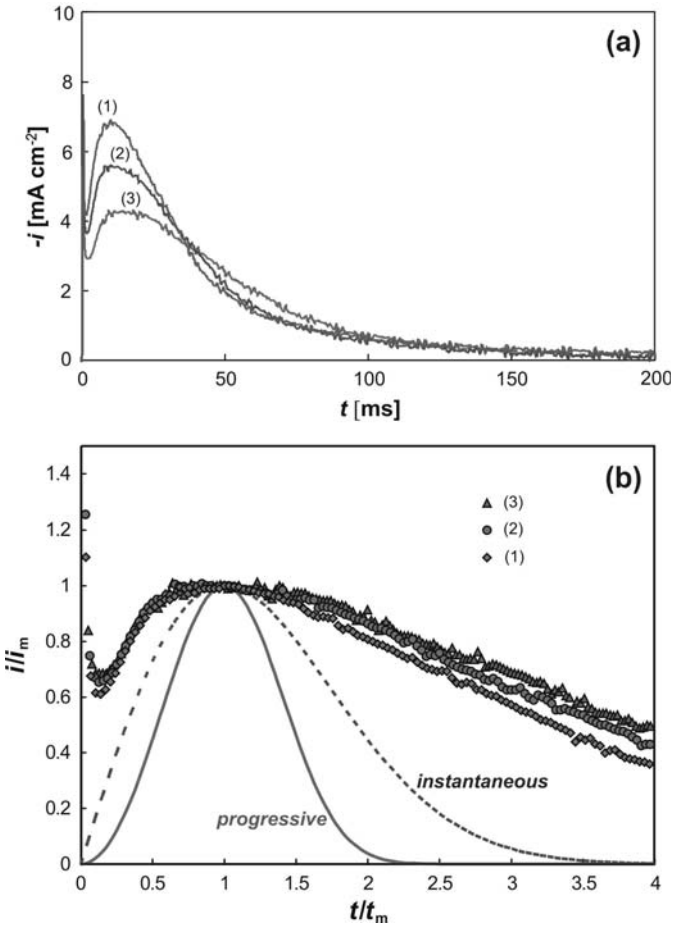

Figure 3. (a): Current transients for Cd UPD on Ag(111) obtained at different underpotentials: (1) ΔE=10mV; (2) ΔE=20mV; (3) ΔE=30mV; (initial underpotential ΔE_i=125mV). (b): i/i_m vs. t/t_m plot of the transients of (a) and the theoretical transients according to the classical models for progressive and instantaneous 2D nucleation (10).

Figure 4(a) presents anodic stripping curves obtained after extended polarization at underpotential ΔE=70mV. The changes of the striping peaks and the shift of the stripping peak D_3 with increasing polarization time t_p indicate the occurrence of some surface transformations. At t_p>30s the corresponding stripping charge density Δq does not change significantly with t_p and is limited to the charge density required for the formation of the condensed Cd monolayer (Figure 4(b)). These results show that the condensed monolayer formed by 2D nucleation and growth at ΔE=70mV transforms under conditions of long time polarization to a thin Ag-Cd surface-confined alloy layer. The occurrence of such transformation is supported also by the behavior presented in Figure 5.

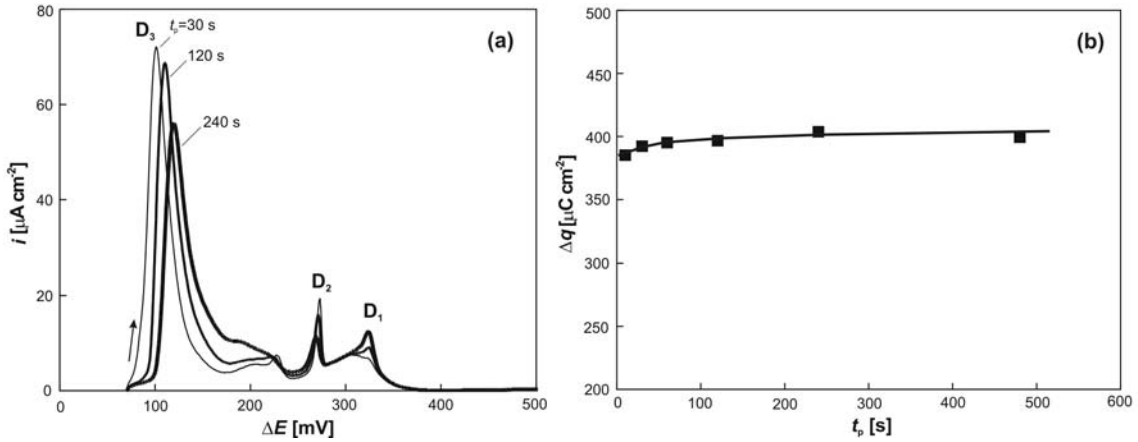

Figure 4. (a): Typical anodic stripping curves obtained in the system Ag(111)/Cd^{2+} after different polarization times t_p at ΔE=70mV (dE/dt=10 mV/s). (b): Dependence of the stripping charge density Δq on t_p.

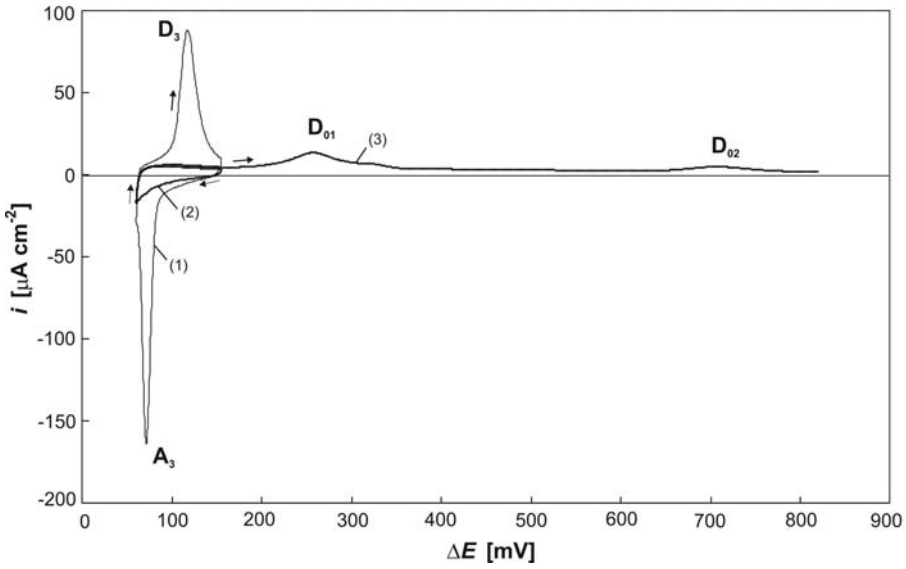

Figure 5. Voltammetric behaviour of the system Ag(111)/Cd^{2+} during the repetitive potential cycling in the UPD range 60mV ≤ ΔE ≤ 155mV (|dE/dt|=10 mV/s). (1): CV after a potential cycling for 1 min. (2): CV after a potential cycling for 60 min. (3): anodic stripping curve after 60 min potential cycling.

The repetitive potential cycling in the range 60mV ≤ ΔE ≤ 155mV for 60 min leads to a complete disappearance of the voltammetric peak pair A_3/D_3 in the cyclic voltammogram (curve (2) in Figure 5) and to an appearance of two new stripping peaks (D_{01} and D_{02}) in the corresponding anodic stripping curve (curve (3) in Figure 5). This behavior confirms the occurrence of a surface alloying and is very similar to that observed in the systems Ag(111)/Pb^{2+} and Ag(111)/Tl^{+} (3,15-20). At lower underpotentials (ΔE<25mV) the Cd UPD in the system Ag(111)/Cd^{2+} involves a significant surface alloy formation, which is reflected in the larger stripping charges and the significant surface roughening observed during the anodic stripping. The kinetics of surface alloy formation occurring in this underpotential range has been analyzed previously on the basis of different theoretical models including Ag-Cd place exchange processes and solid state diffusion (8,21,22).

The System Ag(100)/Cd^{2+}

Figure 6 shows a typical cyclic voltammogram for the system Ag(100)/Cd^{2+}. The voltammogramm exhibits three adsorption(A)/desorption(D) peak pairs located in the underpotential range 40mV<ΔE<350mV. The integration of cyclic voltammogram in the underpotential range 130mV≤ΔE≤350mV corresponding to the peak pair A_1/D_1 reveals a cathodic charge density of $|\Delta q| \approx$ 190 μC/cm^2, which has been previously attributed to the formation of an expanded adlayer with a superlattice structure Ag(100)-c(2×2)Cd (21).

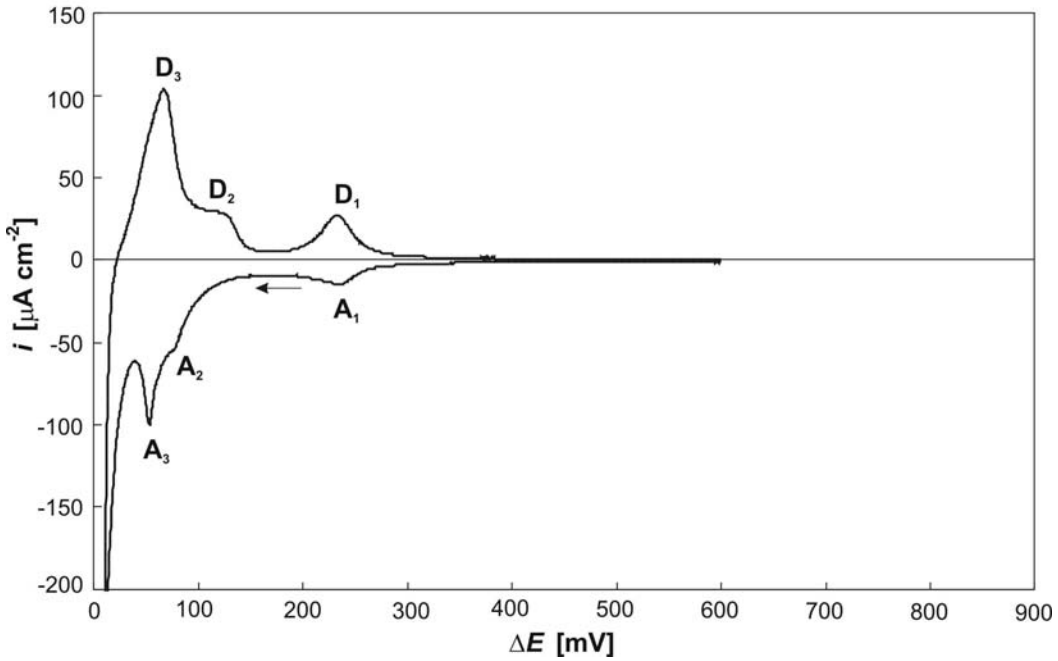

Figure 6. Cyclic voltammogram for Cd UPD in the system Ag(100)/Cd^{2+}(scan rate: $|dE/dt|$ = 10 mV/s).

However, the in situ STM imaging in the potential range 130mV≤ΔE≤180mV shows clearly that the Cd UPD process involves nucleation and slow growth of 2D clusters. Figure 7(a-d) presents a sequence of in situ STM images obtained after stepping the potential from ΔE=400mV (corresponding to a Cd free substrate surface) to ΔE=180mV.

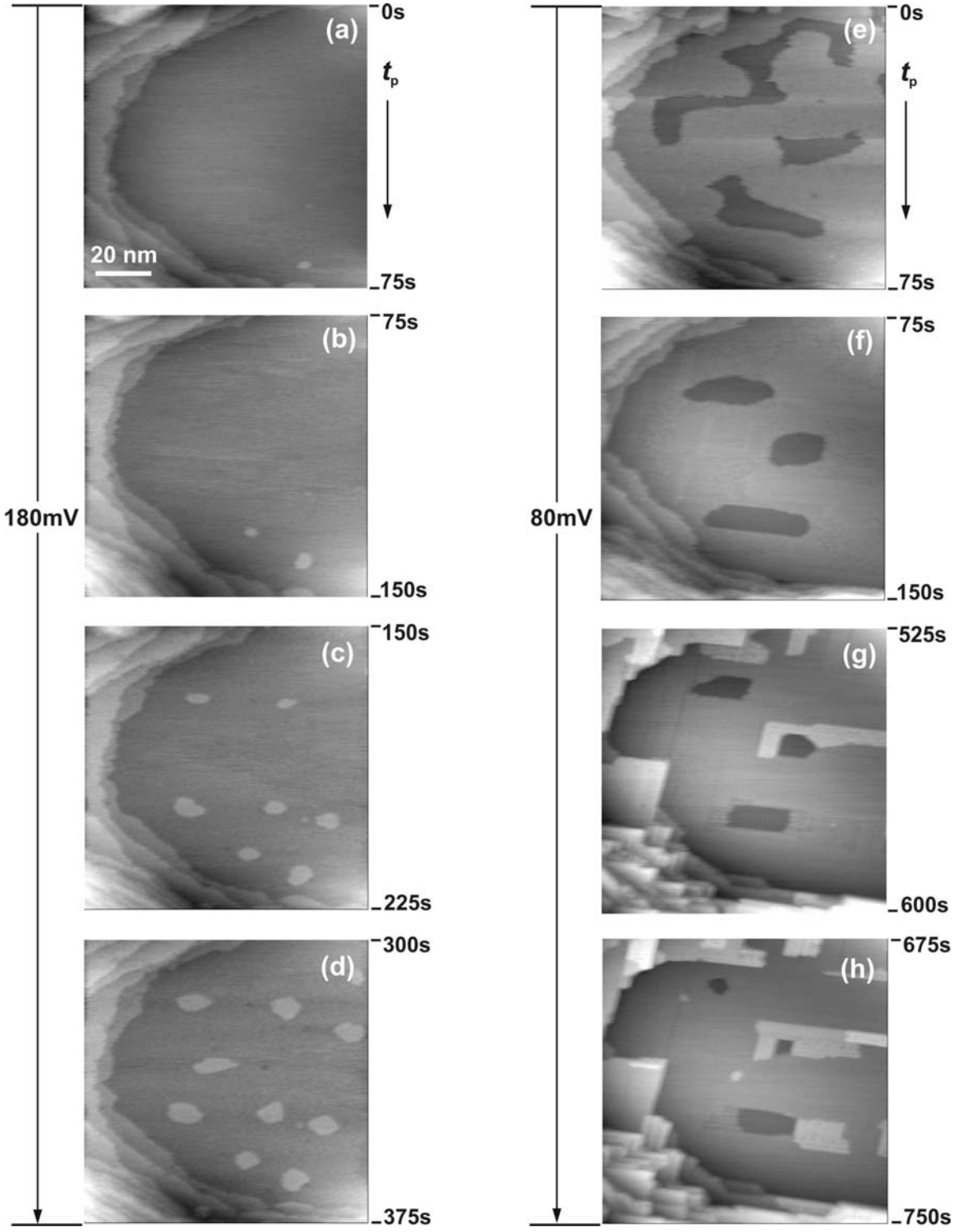

Figure 7. Sequences of in situ STM images obtained during Cd UPD in the system Ag(111)/Cd^{2+} at different polarization conditions. (a-d): Surface topography changes with the polarization time t_p after a potential step from ΔE=400mV to ΔE=180mV. (e-h): Topography evolution of the same surface after stepping the potential from ΔE=180mV to ΔE=80mV.

The first growing 2D cluster appears in the bottom part of the STM image in Figure 7(a). The subsequent STM images in Figure 7(b-d) show the further growth of the first cluster and the appearance and growth of new clusters during the Cd UPD. At the applied underpotential of ΔE=180mV the growth of the clusters is relatively slow, which allows an estimation of the radial growth rate from the sequence of STM images shown in Figure 7(a-d). Figure 8 presents the extracted time dependence of the radius R of first 2D cluster in a R^2 vs. t plot. The observed linear dependence can be attributed to a radial growth rate controlled by surface diffusion. The R-t relationship for the surface diffusion-controlled growth of a single isolated 2D cluster formed at time t_0 after the potential application can be expressed by ( )

$$R = K_{sd} D_{sd}^{1/2} (t - t_0)^{1/2} \qquad [1]$$

where K_{sd} is a constant depending on the applied potential and the structure of condensed monolayer, and D_{sd} represents the surface diffusion coefficient. The intercept of the straight line in Figure 8 reveals a time of birth of the first cluster $t_0 \approx 10\,\mathrm{s}$.

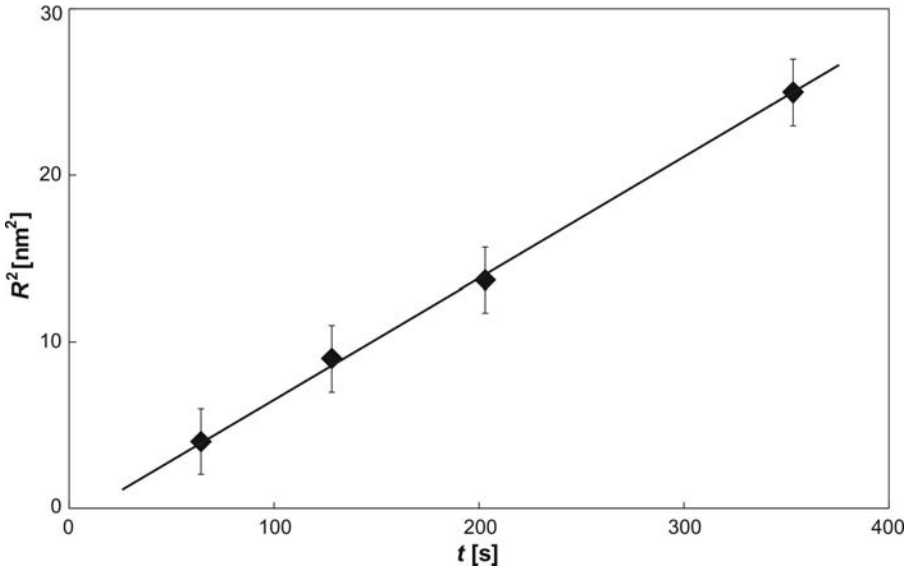

Figure 8. Time dependence of the radius R of the first 2D cluster appearing in the sequence of STM images in Figure 7(a-d).

The sequence of STM images in Figure 7(e-h) presents the topography evolution of the surface shown in Figure 7(a-d) after changing the underpotential from ΔE=180mV to ΔE=80mV. At this underpotential the condensed monolayer begins to complete (Figure 7(e,f)). This process, however, is very slow and long before the full completion of the first monolayer starts the formation of a second and a third monolayers (Figure 7(g,h). Under these conditions the growth morphology is characterized by a multilayer structure and a rectangular form of the growing monolayers reflecting the crystal symmetry of the Ag(100) substrate. Figure 9(a) presents the morphology evolution of the surface in Figure 7(h) after an extended polarization time of t_p=1200s. The STM images in Figures 9(b) and 9(c) show the topography changes of the surface in Figure 9(a) after changing subsequently the polarization potential from ΔE=80mV to ΔE=180mV and ΔE=400mV,

respectively. As seen the dissolution of Cd deposit leads to an appearance of new terraces and a large number of pits. This morphology is characteristic for a dealloying process and indicates the occurrence of a surface alloying during extended polarization at ΔE=80mV.

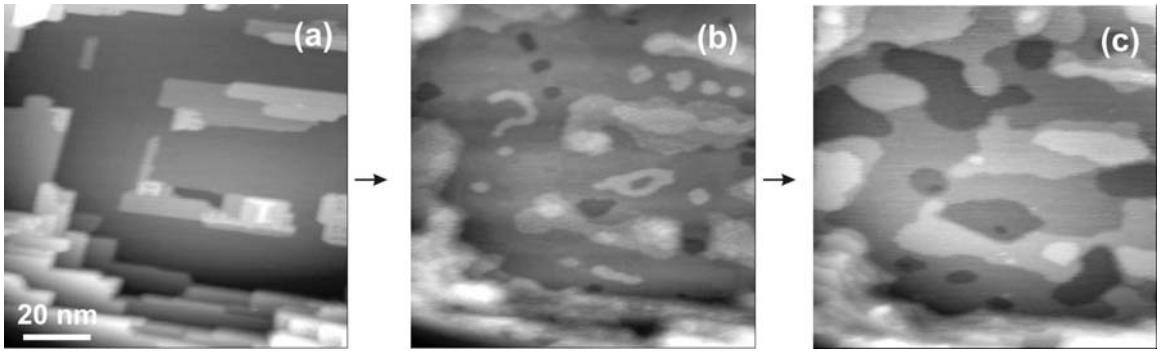

Figure 9. (a): In situ STM image obtained in the system Ag(100)/Cd^{2+} after polarization at ΔE=80mV for t_p=1200s. (b): Topography changes of the surface in (a) after polarization at ΔE=180mV for t_p=140s. (c): Topography changes of the surface in (b) after polarization at ΔE=400mV for t_p=180s.

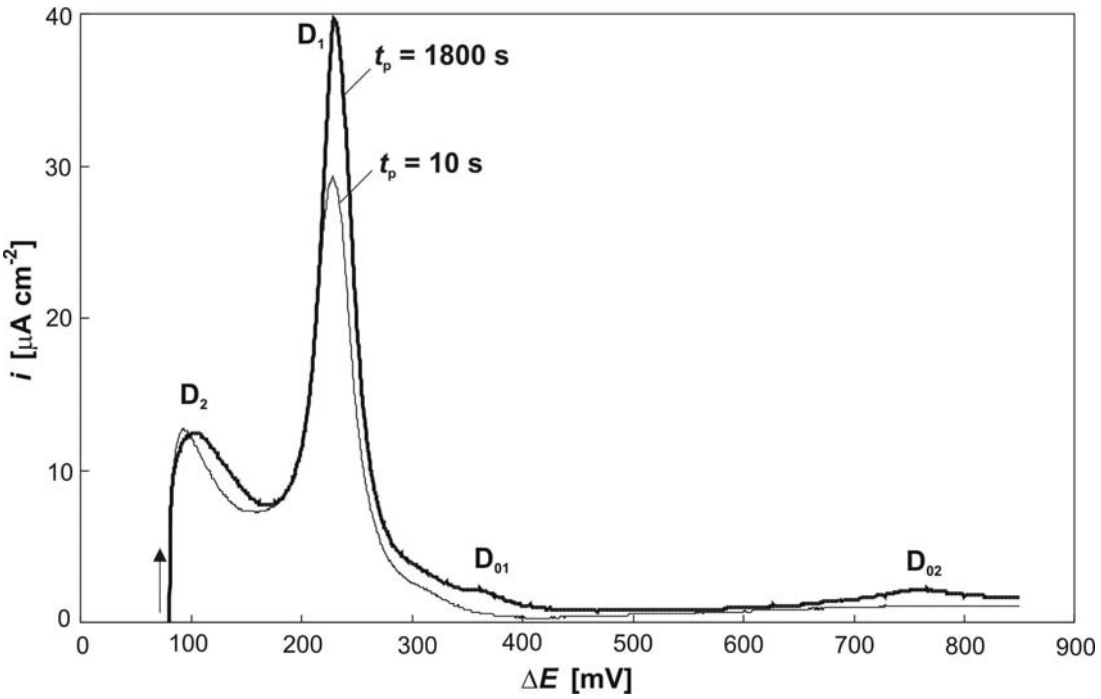

Figure 10. Anodic stripping curves obtained in the system Ag(100)/Cd^{2+} after polarization at ΔE=80mV for t_p=10s and t_p=1800s, respectively.

The occurrence of surface alloying is supported also by the stripping curve obtained after polarization at ΔE=80mV for t_p=1800s (Figure 10). The striping curve shows an appearance of two new stripping peaks D_{01} and D_{02} at relatively larger underpotentials. This behavior is very similar to that observed in the system Ag(111)/Cd^{2+} (cf. Figure 5) and is typical for a dealloying process (8,19,20).

Conclusions

The presented in situ STM studies show clearly that the UPD of Cd on Ag(111) and Ag(100) surfaces involves a formation of condensed monolayers by 2D nucleation and growth. The results reveal that on Ag(111) the UPD process starts at underpotentials ΔE<400mV with a formation of an expanded $Ag(111)-(\sqrt{3}\times\sqrt{19})R23.4°$ adlayer. In the potential range 50mV<ΔE<80mV this adlayer transforms by 2D nucleation and growth to a condensed close packed monolayer. By long time polarization in this potential range the condensed monolayer undergoes transformations involving place exchange processes and leading to formation of a surface-confined Ag-Cd alloy. In contrast to the system Ag(111)/Cd^{2+}, in situ STM studies in the system Ag(100)/Cd^{2+} show 2D nucleation and growth of clusters at higher underpotentials (130≤ΔE≤180mV). The radial growth rate of the clusters extracted from the STM images indicates surface diffusion-controlled growth kinetics. Similarly as in the system Ag(111)/Cd^{2+}, the extended polarization at a lower underpotential of ΔE=80mV leads to a surface alloying, which is reflected in the observed changes of the anodic stripping curves and the surface topography.

Acknowledgments

The financial support of the Forschungszentrum Jülich GmbH, the Universidad Nacional del Sur, and the Deutsche Akademische Austauschdienst (DAAD) is gratefully acknowledged.

References

1. E. Budevski, V. Bostanov and G. Staikov, *Ann. Rev. Mat. Sci.*, **10**, 85 (1980).
2. E. Budevski, in *Comprehensive Treatise of Electrochemistry*, B. E. Conway, J. O'M. Bockris, E. Yeager, S. U. M. Khan and R. E. White, Editors, p. 399, Vol. 7, Plenum Press, New York (1983).
3. E. Budevski, G. Staikov and W. J. Lorenz, *Electrochemical Phase Formation and Growth - An Introduction to the Initial Stages of Metal Deposition*, VCH, Weinheim (1996).
4. G. Staikov, W. J. Lorenz and E. Budevski, in *Imaging of Surfaces and Interfaces (Frontiers in Electrochemistry)*, P. Ross and J. Lipkowski, Editors, p. 1, Vol. 5, Wiley-VCH, New York, Weinheim (1999).
5. J. L. Stickney, in *Electroanalytical Chemistry*, A. J. Bard and I. Rubinstein, Editors, p. 75, Vol. 21, Marcel Dekker, New York (1999).
6. J. L. Stickney, in *Advances in Electrochemical Science and Engineering*, R. C. Alkire and D. M. Kolb, Editors, p. 1, Vol. 7, Wiley-VCH, Weinheim (2001).
7. S. García, D. R. Salinas, C. E. Mayer, W. J. Lorenz and G. Staikov, *Electrochim. Acta*, **48**, 1279 (2003).
8. S. García, D. R. Salinas and G. Staikov, *Surf. Sci.*, **576**, 9 (2005).
9. M. Fleischmann and H. R. Thirsk, in *Advances of Electrochemistry and Electrochemical Engineering*, P. Delahay, Editor, p. 123, Vol. 3, John Wiley & Sons (1963).
10. J. A. Harrison and H. R. Thirsk, in *Electroanalytical Chemistry*, A. J. Bard, Editor, p. 67, Vol. 5, Marcel Dekker, New York (1971).

11. M. Arbib, B. Zhang, V. Lazarov, D. Stoychev, A. Milchev and C. Buess-Hermann, *J. Electroanal. Chem.*, **510**, 67 (2001).
12. F. C. Frank, *Proc. Roy. Soc.*, **A201**, 586 (1950).
13. R. D. Armstrong and J. A. Harrison, *J. Electrochem. Soc.*, **116**, 328 (1969).
14. R. Philipp and U. Retter, *Thin Solid Films*, **259**, 59 (1995).
15. E. Schmidt and H. Siegenthaler, *J. Electroanal. Chem.*, **150**, 59 (1983).
16. T. Vitanov, A. Popov, G. Staikov, E. Budevski, W. J. Lorenz and E. Schmidt, *Electrochim. Acta*, **31**, 981 (1986).
17. N. Dimitrov, A. Popov, D. Kashchiev, T. Vitanov and E. Budevski, *Electrochim. Acta*, **36**, 1259 (1991).
18. N. Dimitrov, A. Popov, T. Vitanov and E. Budevski, *Electrochim. Acta*, **36**, 2077 (1991).
19. D. Carnal, P. I. Oden, U. Müller, E. Schmidt and H. Siegenthaler, *Electrochim. Acta*, **40**, 1223 (1995).
20. R. Widmer and H. Siegenthaler, *J. Electrochem. Soc.*, **151**, E238 (2004).
21. H. Bort, K. Jüttner, W. J. Lorenz and G. Staikov, *Electrochim. Acta*, **28**, 993 (1983).
22. R. Vidu, N. Hirai and S. Hara, *Phys. Chem. Chem. Phys.*, **3**, 3320 (2001).